Physics Letters A 375 (2011) 2122–2128

Contents lists available at ScienceDirect

Physics Letters A

www.elsevier.com/locate/pla

Conducting properties of classical transmission lines with Ornstein–Uhlenbeck type disorder

E. Lazo [a,*], E. Diez [b]

[a] Departamento de Física, Facultad de Ciencias, Universidad de Tarapacá, Arica, Chile
[b] Departamento de Física Fundamental, Universidad de Salamanca, Salamanca, E-37008, Spain

ARTICLE INFO

Article history:
Received 27 December 2010
Received in revised form 18 February 2011
Accepted 20 February 2011
Available online 24 February 2011
Communicated by R. Wu

Keywords:
Localization–delocalization transition
Disordered electrical circuits
Long-range correlations
Ornstein–Uhlenbeck process

ABSTRACT

In this work we study the behavior of bands of extended states and localized states which appear in classical disordered electrical transmission lines, when we use a ternary map and the Ornstein–Uhlenbeck process to generate the long-range correlated disorder, instead of using the Fourier filtering method. By performing finite-size scaling we obtain the asymptotic value of the map parameter b in the thermodynamic limit in a selected range of values of the parameters γ and C of the Ornstein–Uhlenbeck process. With these data we obtain the phase diagrams which separate the localized states from the extended states. These are the fundamental results of this article.

1. Introduction

According to the theory of Anderson localization and based on analytical and numerical evidence, the quantum wave function of an electron in a one-dimensional disordered system is localized even for infinitesimal amount of disorder [1,2].

Recently, analytical and numerical studies have shown that in one-dimensional systems the electron wave function can be delocalized when we consider disorder with short-range [3–7] and long range [8–17] correlations.

On the other hand, from the scaling theory [18] we known that in the thermodynamic limit, an infinitesimal disorder can cause localization of all states in one and two-dimensional systems. The delocalization mechanism of the long-range correlations in the disorder can be clearly seen in a work by Díaz et al. [19].

From the experimental point of view, it was shown that the correlation in the disorder is responsible for delocalization in some specific cases: microwave propagation through disordered waveguides [20], subterahertz response of superconducting multilayer [21] and in semiconductor superlattices with intentional disorder [22].

Recently, the introduction of long-range correlation in disordered classical transmission lines (TL) has been studied by Lazo and Diez [23] using a ternary map considering the Fourier filtering method (FFM) [24] to generate the long-range correlated sequence. The phase diagram of the transition from non-conducting to conducting state of the TL in the thermodynamic limit was obtained by performing finite-size scaling.

In this work we study the localization effect which appear in TL with long-range correlated disorder in the distribution of capacitances $\{C_j\}$, using a ternary map and using the Ornstein–Uhlenbeck (OU) process to generate the correlated sequence. To study the phase transition in the thermodynamic limit we apply the scaling theory.

The now called Ornstein–Uhlenbeck process was introduced in essence by Langevin in 1908 in his paper on Brownian motion [25]. The mathematical formalization of this process was initiated three decades later by Uhlenbeck and Ornstein [26] and followed by works by Chandrasekhar [27] and Wang and Uhlenbeck [28]. Actually, the OU process is well established and is incorporated in standard textbook [29].

Using the OU sequence we generate the symmetric ternary map by means of the map parameter b, which adjust the occupancy probability of each possible value of the capacitances $C_j = \{C_A, C_B, C_C,\}$.

In general, the dynamics of the TL as a function of the frequency ω has a very similar behavior in comparison with the behavior of the 1D tight-binding quantum systems as a function of the eigenenergy E. If the sequence of capacitance values is totally at random (white noise), the disordered TL is in the non-conducting state for every frequency ω. For periodic distribution of capacitances, the TL presents a structure of allowed and forbidden bands as a function of the frequency ω. For short-range correlated disorder in the distribution of capacitances, the TL is in the non-

* Corresponding author.
E-mail address: elazo@uta.cl (E. Lazo).

0375-9601/$ – see front matter
doi:10.1016/j.physleta.2011.02.049

conducting state for every frequency ω. However, for certain finite number n of specific values of the frequency: $\omega_1, \omega_2, \omega_3, \ldots, \omega_n$, is possible to find the TL in the conducting state. For long-range correlated disorder in the distribution of capacitances, it is possible to find bands of allowed frequencies ω in between forbidden bands, for which the TL is in the conducting state [23].

When we use the OU process to introduce the long-range correlation in the distribution of capacitances by means of the ternary map, determined by the map parameter b, the TL changes its properties and we can find a transition from the localized to extended state for a fixed system size N. This implies the existence of a critical value of the map parameter $b = b_c$ for specific values of the parameters γ and C which defines the OU process.

By performing finite-size scaling we obtain the asymptotic value of the parameter b in the thermodynamic limit for given γ and C. With these data we present below three phase diagrams for the ternary model, separating the localized state from the extended one, namely: (γ, b_c) and (C, b_c) for independent variation of γ and C, and (γ, b_c) for the limit case, where $C = (\varepsilon\gamma)^2$, with $\varepsilon = 1$ and $\gamma \to \infty$. In addition, we have shown that changing the kind of long-range correlated sequence from the FFM (used in Ref. [23] and which depends on a single parameter) to the OU process (which depends on two parameters), maintains the dynamics of bands and gaps but in a richer way due to the increased number of parameters, but also find important differences in the shape of the phase diagrams of the various cases studied. These are the fundamental results of this article.

2. Model and method

Let us consider electrical circuits of classical impedances Z_j and g_j as shown in Fig. 1. Application of Kirchhoff's Loop Rule to three successive unit cells leads to the following equation

$$(Z_j + g_{j-1} + g_j)I_j - g_{j-1}I_{j-1} - g_j I_{j+1} = 0 \tag{1}$$

where I_{j-1}, I_j and I_{j+1} are the currents circulating in the $(j-1)$-th, j-th and $(j+1)$-th cell, respectively.

2.1. Disordered dual transmission line

Using the horizontal impedances being equal capacitances with $Z_j = (\frac{-i}{\bar{\omega}C_j})$ and vertical impedances being equal to inductances with $g_j = (i\bar{\omega}L_j)$, Eq. (1) can be written

$$\left(L_{j-1} + L_j - \frac{1}{\bar{\omega}^2 C_j}\right)I_j - L_{j-1}I_{j-1} - L_j I_{j+1} = 0 \tag{2}$$

where $\bar{\omega}$ is the frequency. This equation describes the behavior of TL with diagonal and non-diagonal disorder. For the case with only diagonal disorder, we put $L_j = L_0, \forall j$ and we write $C_j = C_0\alpha_j$. In this case, dividing by $i\bar{\omega}L_0$, Eq. (2) can be written as,

$$d_j I_j - I_{j-1} - I_{j+1} = 0 \tag{3}$$

where

$$d_j = \left(2 - \frac{1}{\omega^2\alpha_j}\right) \tag{4}$$

Here we have used $\omega = \bar{\omega}\sqrt{L_0 C_0}$, defining in this way the frequency ω measured in units of $\frac{1}{\sqrt{L_0 C_0}}$.

Using the following definition: $\gamma_j = \frac{I_{j+1}}{I_j}$, Eq. (3) can be written as a recurrence equation

$$\gamma_j = d_j - \frac{1}{\gamma_{j-1}} \tag{5}$$

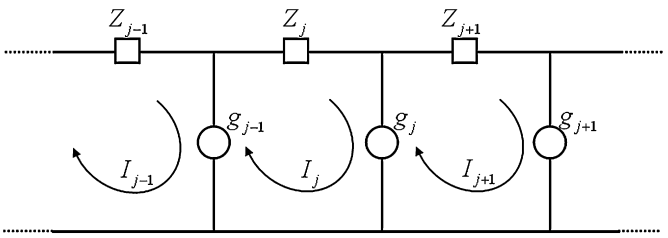

Fig. 1. Segment of an infinite electric circuit of classical impedances.

In order to study the transition from localized to extended states in disordered TL, we use the Lyapunov exponent formalism. The Lyapunov exponent $\lambda(\omega)$ is a function of the frequency ω and in this case can be defined as

$$\lambda(\omega) = \lim_{N\to\infty} \frac{1}{N}\sum_{j=1}^{N} \ln\left|\frac{I_{j+1}}{I_j}\right| \tag{6}$$

Using the γ_j definition, we can write $\lambda(\omega)$ in the following form

$$\lambda(\omega) = \lim_{N\to\infty} \frac{1}{N}\sum_{j=1}^{N} \ln|\gamma_j| \tag{7}$$

The Lyapunov exponent $\lambda(\omega)$ is a suitable tool to describe conduction properties through the TL, because it is related to the exponential decrease of the electric current function I_j. The localization length $\xi(\omega)$ is defined as the inverse of the Lyapunov exponent:

$$\xi(\omega) = \frac{1}{\lambda(\omega)} \tag{8}$$

This relation gives the single value of $\xi(\omega)$ only for the infinite system size $N \to \infty$. However, when N is finite, the calculated result of relation (8) – denoted as ξ_N – depends on the specific form of the sequence of capacitances $\{C_j\}$. To obtain a typical value of ξ_N for a given N, we take the mean of ξ_N over 5000 samples from which we define the normalized localization length $\Lambda = \frac{\xi_N}{N}$ on the system size N. In this work we use the localization length Λ to characterize extended or localized states using the following criteria for a fixed number of cells N in the transmission lines and a specific frequency ω: if $\Lambda(\omega) \geqslant 1$ the TL is in the extended state because $\xi_N \geqslant N$, and if $\Lambda(\omega) < 1$, the TL is in the localized state because $\xi_N < N$. The localized and extended states in disordered TL are analogous to the localized and extended states in 1D disordered quantum system.

In all our calculations, the possibility of a phase transition from localized to extended states in the TL is studied for a fixed frequency $\omega = 3.5$. However, in the thermodynamic limit, $N \to \infty$, we have verified that the results do not change when we use a different frequency $\omega' \neq \omega$.

2.2. Long-range correlated disorder

In this work we use the Ornstein–Uhlenbeck process to generate the long-range correlated sequence of capacitances $\{C_j\}$ by means of the ternary map. The OU process is defined by the following differential equation:

$$\frac{dx}{dt} = -\gamma x(t) + \sqrt{C}\eta(t) \tag{9}$$

where γ is the viscosity coefficient and C is the diffusion coefficient. $\eta(t)$ is a Gaussian white noise generated by the Box–Muller process with the following properties:

$$\langle\eta(t)\rangle = 0, \qquad \langle\eta(t)\eta(t+\tau)\rangle = \delta(\tau)$$

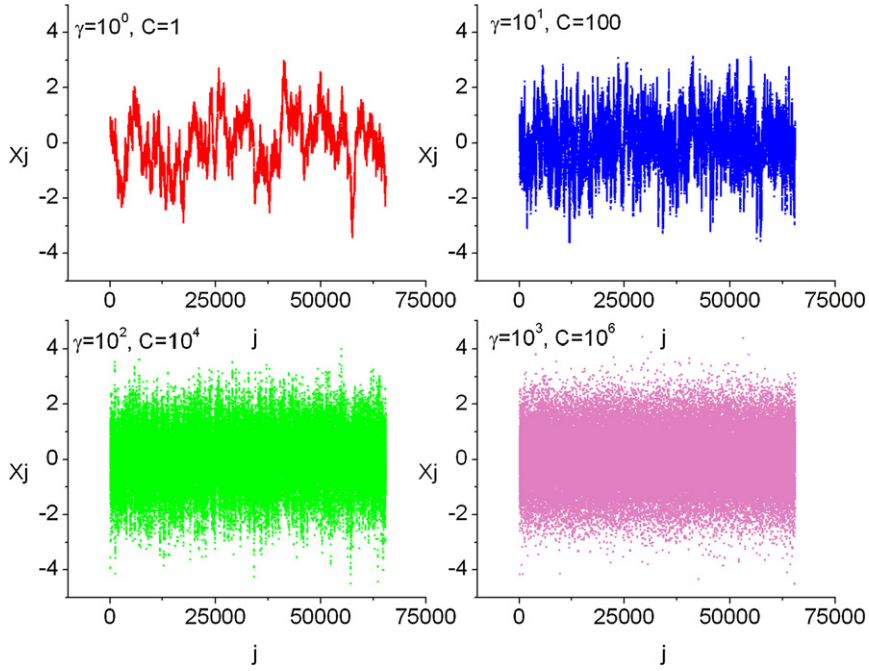

Fig. 2. Ornstein–Uhlenbeck sequences for four different values of the parameter $\gamma = \{1, 10, 10^2, 10^3\}$, with $C = (\varepsilon\gamma)^2$ using $\varepsilon = 1$ (limit case). The OU sequence gradually evolve, as $\gamma \to \infty$, into the Gaussian white noise process, showing in this way that the long-range correlation is diminishing as $\gamma \to \infty$.

The OU sequence $x(t)$ has the following properties:

$$\langle x(t)\rangle = x_0 e^{-\gamma t}, \qquad \langle x(t)x(t+\tau)\rangle = \frac{C}{2\gamma} e^{-\gamma\tau}$$

To generate the OU sequence we use the exact numerical simulation given by Gillespie [30]. In this method, Eq. (9) can be discretized by means of the following equation relating $x(t)$ in two different times $t_1 = t$ and $t_2 = (t + \Delta t)$:

$$x(t + \Delta t) = \mu x(t) + \sigma_x n_1(t)$$

where the parameters μ, σ_x are defined as a function of the parameters γ and C of the OU process (9) in the following form

$$\mu = e^{-\gamma\Delta t}$$

$$\sigma_x^2 = \left(\frac{C}{2\gamma}\right)(1 - \mu^2)$$

Using the Box–Muller algorithm we calculate $n_1(t)$ in the following way

$$n_1(t) = s\cos\theta$$

where

$$s^2 = 2\ln\frac{1}{r_1}, \qquad \theta = 2\pi r_2$$

and r_1, r_2 are uniform random numbers defined in the interval $[0, 1]$. As a final numerical step, we normalize the sequence $\{x_j\}$ to obtain zero average, $\langle x_j\rangle = 0$ and the variance is set to unity. With this normalized sequence $\{x_j\}$ we build the symmetric ternary model, which is generated by means of a transformation which maps the elements of the normalized long-range correlated sequence $\{x_j\}$ into three different values of capacitances $C_j = \{\alpha_A, \alpha_B, \alpha_C\}C_0$, by means of the map parameter b.

To show the long-range correlated behavior of the OU sequence, we study the behavior of the sequences in the limit case, when the parameters $\gamma \to \infty$ and $C \to \infty$, in such a way that $\frac{\sqrt{C}}{\gamma} = \varepsilon$ stays constant. The final sequence $\{x_j\}$ will approach $\varepsilon \times$ (Gaussian white noise) [30]. Fig. 2 shows the sequence $\{x_j\}$ for four values of the parameter $\gamma = \{1, 10, 10^2, 10^3\}$, considering $\varepsilon = 1$ and $C = (\varepsilon\gamma)^2$. We clearly can see that the OU sequence evolves, as $\gamma \to \infty$, into the Gaussian white noise. The linear fit by least squares of the log–log plot of the power spectrum $PS(f)$ as a function of the frequency f (not shown) allows writing the relation $PS(f) = f^{-m}$. The slope m approaches zero, $m \to 0$, for $\gamma \to \infty$, which shows that the sequence of OU is losing its long-range correlation for increasing values of γ.

2.3. The symmetric ternary model

Using the sequence $\{x_j\}$ generated by OU process and writing the capacitances in the form $C_j = C_0\alpha_j$, the sequence of capacitances $\{C_j\}$ of the ternary model is obtained by means of the following map,

$$\alpha_j = \begin{cases} \alpha_A & \text{if } x_j < -b \\ \alpha_C & \text{if } -b \leqslant x_j \leqslant b \\ \alpha_B & \text{if } x_j > b \end{cases} \tag{10}$$

where $b > 0$ is the map parameter, which adjust the occupancy probability of each possible value of the capacitances $C_j = \{C_A, C_B, C_C,\}$. The ternary map (10) changes the correlation properties of the original OU sequence $\{x_j\}$, and therefore, the correlation of the sequence $\{C_j\}$ is not properly quantified by the OU parameters γ and C, which define the original correlated sequence $\{x_j\}$.

The metal–insulator transition in binary and ternary symmetrical model for 1D tight-binding systems has been studied in Refs. [9,11] and [14], respectively. In electrical transmission lines, the transition from localized state to extended one, using the Fourier filtering method and the ternary map to generate long-range correlation, has been studied in Ref. [23].

2.4. The finite-size scaling

Using the finite-size scaling [31–33], we can identify the critical points of finite systems. Finite-size scaling characterizes the scaling

behavior of thermodynamic quantities of finite system near a critical point. The basic idea of the finite-size scaling is the following. Let us consider an observable Q of a finite system which is a function of a critical parameter P and system size N. When N is much larger that the microscopic length scale and P is in the vicinity of the critical point P_c, the observable $Q(P,N)$ can be written in the finite-size scaling form [34], $Q(P,N) = N^{\frac{\lambda}{\nu}} F_Q(tN^{\frac{1}{\nu}})$, where $t = (P - P_c)/P_c$ is the reduced critical parameter and λ is the critical exponent of the observable Q and ν is the critical exponent of the correlation length $\xi = \xi_0 t^{-\nu}$. The critical point can be find using finite-size scaling. At critical point $P = P_c$, the reduced critical parameter t goes to zero, $t = 0$, and we can write $Q(P_c,N)N^{-\frac{\lambda}{\nu}} = F_Q(0)$, where the finite-size scaling function $F_Q(0)$ is constant and independent of the system size N. In the plot of $Q(P,N)N^{-\frac{\lambda}{\nu}}$ *versus* P, all curves of different system sizes converge to the critical point $[P_c, F_Q(0)]$ which at the same time is a fixed point. On the contrary, the existence of a fixed point indicates the existence of a critical point. In this way, the critical point can be found from the system size dependence of the observable. Taking the logarithm of $Q(P,N)$, we obtain $\ln Q(P,N) = \frac{\lambda}{\nu}\ln N + \ln F_Q(tN^{\frac{1}{\nu}})$. At critical point, $P = P_c$, $t = 0$ and $F_Q(tN^{\frac{1}{\nu}}) \to F_Q(0)$, where the finite-size scaling function $F_Q(0)$ is a constant. In this case, $\ln F_Q(tN^{\frac{1}{\nu}})$ becomes a constant and, consequently, $\ln Q(P_c,N)$ becomes a straight line with respect to $\ln N$. When the system is away from the critical point ($P \neq P_c$ and $t \neq 0$), the plot of $\ln Q(P,N)$ *versus* $\ln N$, does not represent a straight line, because the function $F_Q(tN^{\frac{1}{\nu}})$ depends on the system size N and on the critical parameter P through the relation $t = (P - P_c)/P_c$.

In this work we use the finite-size scaling considering as the observable Q, the normalized localization length Λ, namely, $Q = \Lambda$. In general, $\Lambda = \Lambda(\omega, b, \gamma, C, N)$, depends on the frequency ω, the ternary map parameter b, the OU parameters γ and C, and the system size N.

Considering the map parameter b as the critical parameter, i.e., $P = b$, for known values of parameters γ and C and the frequency ω, the fixed point can be found by investigating the dependence of the function $\Lambda(b,N)N^{-\beta}$ of parameter b for different system sizes N. When a fixed point is observed at a certain parameter β, it indicates the existence of a critical point and the parameter β is related to the ratio of critical exponents, i.e., $\beta = \frac{\lambda}{\nu}$. To characterize the scaling behavior of $\Lambda(b,N)$ for a finite system size near critical point, we will use the finite-size scaling. To do that, for a fixed OU parameters γ and C, we can write the scaling relation

$$\Lambda(b_c,N)N^{-\beta} = F_\Lambda(0) \tag{11}$$

where β is the critical exponent. In this way, varying the critical exponent β we can find the fixed points b_c. In addition, the critical point $b = b_c$ can be found studying the system size dependence of $\ln\Lambda(b,N)$ for different values of the map parameter b. At critical point, $b = b_c$ ($t = 0$), in this case $\ln\Lambda(b_c,N)$ becomes a straight line with respect to $\ln N$, because $\ln F_\Lambda(0)$ becomes a constant, namely,

$$\ln\Lambda(b_c,N) = \beta\ln N + \ln F_\Lambda(0) \tag{12}$$

3. Numerical results

3.1. The ternary map

In this work we study the localization properties of disordered TL when the long-correlated disorder is obtained from the OU process using the symmetric ternary map (10). In all numerical calculations, the possibility of a phase transition in the thermodynamic limit from localized to extended state is investigated for a fixed frequency $\omega = 3.5$, using the ternary map parameter b as the critical parameter, were $b = b(\gamma, C)$ is a function of the OU parameters γ and C. As a consequence, we study the behavior of the observable $\Lambda(b,N)$ on the system size N, for fixed γ and C values. The critical point $b = b_c$, permits us to discriminate between localized and extended states. Specifically, we study two kind of behavior: i) γ and C vary independently and ii) the limit case: $C = (\varepsilon\gamma)^2$ and $\varepsilon = 1$, with $\gamma \to \infty$.

i) γ and C vary independently.

In this case we study the behavior of the TL with long-range correlated disorder considering a very limited range of values of the parameters γ and C. In addition, γ and C vary independently. Specifically, we study two cases: a) $\gamma = 0.9$ fixed and C variable, and b) $C = 0.3$ fixed and γ variable.

Case a) $\gamma = 0.9$ fixed and C variable.

To characterize the scaling behavior of $\Lambda(b,N)$ for finite system size near critical point, we use the finite-size scaling relations (11) and (12) for given parameters γ and C. At critical point $b = b_c$, the reduced critical parameter t goes to zero ($t = 0$), therefore $\ln\Lambda(b_c,N)$ becomes a straight line with respect to $\ln N$, because $\ln F_\Lambda(0)$ becomes a constant. Using relation (12), Fig. 3 shows that the best linear fit for $\gamma = 0.9$ and $C = 0.04$, occurs for $b_c = 4.16$. In addition, using relation (11), the inset of Fig. 3 shows the behavior of $\Lambda(b,N)N^{-\beta}$ versus the map parameter b, for a specific critical exponent β_0, for $\gamma = 0.9$ and $C = 0.04$, for various system size ranging from $N = 2.5\times10^5$ to $N = 1.5\times10^6$. Here we can see the presence of a fixed point at the same place of the critical point $b_c = 4.16$ showed in Fig. 3. In this fixed point $b_c = 4.16$ a convergence of all curves for different systems sizes N can be observed. The existence of a fixed point indicates the existence of a critical point.

In this Letter, we have found every critical point $b_c(\gamma, C)$ at thermodynamic limit using relation (12). With these data we have found the phase diagram (C, b_c), showed in Fig. 4, which separate localized states from extended states for the case $\gamma = 0.9$ fixed and C variable. This is the most important result for this case.

Additionally, we study the behavior of the normalized localization length $\Lambda(b)$ as a function of the map parameter b for fixed system size N and $\gamma = 0.9$, for different values of the parameter C. In the inset of Fig. 4 we show this behavior for $\omega = 3.5$, system size $N = 40\,000$, $\gamma = 0.9$ and C ranging from $C = 0.001$ to $C = 0.15$. The generic behavior is the following: for each C value, $\Lambda(b)$ is a growing function of the map parameter b until it reaches a particular value, which we call saturation point $b = b_s(C,N)$, whose value depends on the system size N and the value of the parameter C. For $b \geqslant b_s$, $\Lambda(b)$ is practically independent of b. We can also observe that for increasing values of the parameter C, diminishes the value of the saturation point b_s and then, b_s seems not to change. In concordance with the behavior obtained for the saturation point $b_s(C,N)$, the critical value b_c at thermodynamic limit (the phase diagram of Fig. 4) diminishes for increasing values of the parameter C and then b_c does not change.

Case b) $C = 0.3$ fixed and γ variable.

Using relation (12), we have found every critical point $b_c(\gamma, C)$ at thermodynamic limit. Fig. 5 shows the phase diagram (γ, b_c), which is the most important result for this case. This phase diagram is very different from phase diagram of the case a), because now b_c is a growing function of γ, until b_c becomes a constant.

In this case we also study the normalized localization length $\Lambda(b)$ as a function of the map parameter b for $\omega = 3.5$, fixed sys-

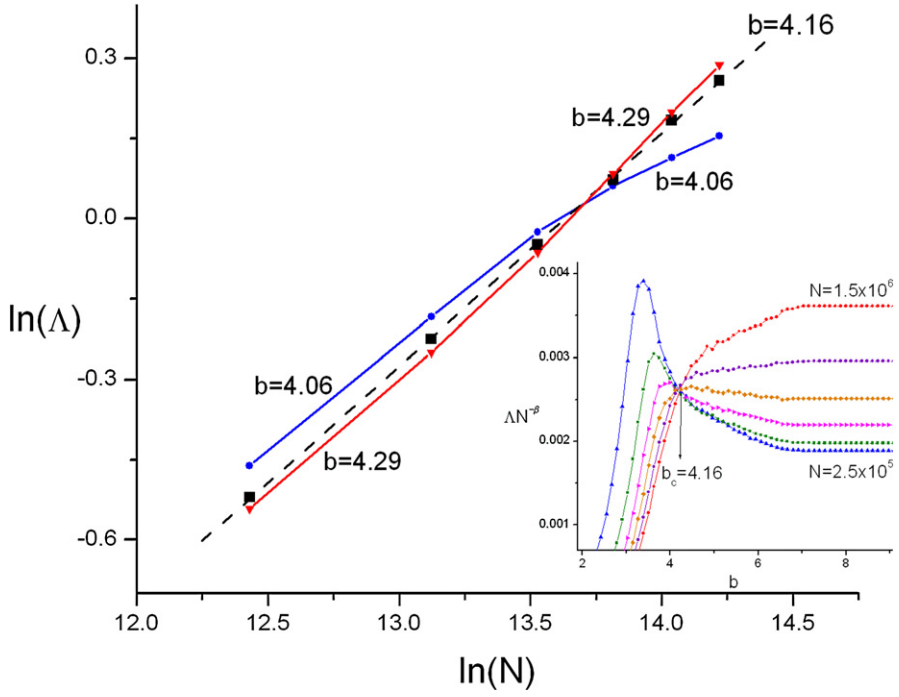

Fig. 3. Scaling plot of $\ln(\Lambda(b,N))$ versus $\ln(N)$ for $\omega = 3.5$, $\gamma = 0.9$ and $C = 0.04$ for N ranging from $N = 2.5 \times 10^5$ to $N = 1.5 \times 10^6$, for different b values. The best straight line (with a correlation coefficient $R \geqslant 0.9999$) occurs when the critical point is $b_c = 4.16$. The inset shows the scaling plot of $\Lambda(b,N)N^{-\beta}$ versus the map parameter b. For a specific critical exponent β_0, a fixed point, $b_c = 4.16$, appears, where all curves of different system sizes converge. Both scaling plots give the same numerical result.

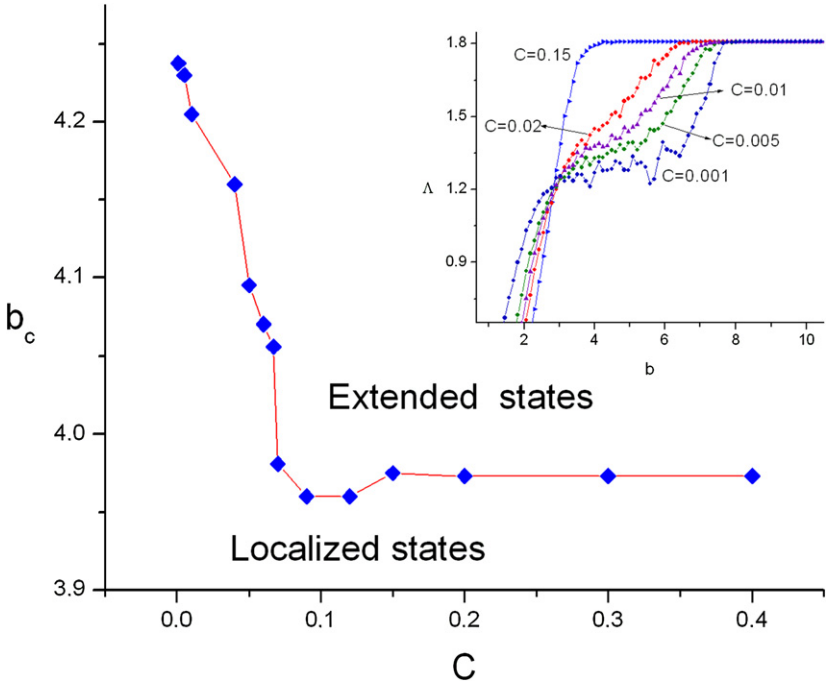

Fig. 4. Phase diagram (C, b_c) separating localized states from extended states in the thermodynamic limit in terms of the map parameter $b_c(\infty)$ for $\gamma = 0.9$ as a function of the parameter C. The inset shows the normalized localization length $\Lambda(b)$ as a function of the map parameter b for $\omega = 3.5$, $N = 40\,000$ and $\gamma = 0.9$, for C going from $C = 0.001$ to $C = 0.15$.

tem size N and $C = 0.3$ for different values of the γ parameter. In the inset of Fig. 5 we show this behavior for $N = 40\,000$, $C = 0.3$ and γ ranging from $\gamma = 0.001$ to $\gamma = 4.0$. Now, the generic behavior is the following: for each γ value, $\Lambda(b)$ is a growing function of the map parameter b until the corresponding saturation point $b = b_s$ appears. This saturation point b_s has a specific value depending on the system size N and the value of the parameter γ, namely, $b_s = b_s(\gamma, N)$. For $b \geqslant b_s$, $\Lambda(b)$ is practically independent of b. We can also observe that for increasing values of the parameter γ, increases the value of b_s and then, b_s seems not to change. This behavior is very different from the case $\gamma = 0.9$ fixed and C variable, studied in the case a). In concordance with the behavior obtained for the saturation point $b_s(\gamma, N)$, the critical value b_c at thermodynamic limit (the phase diagram of Fig. 5) increases

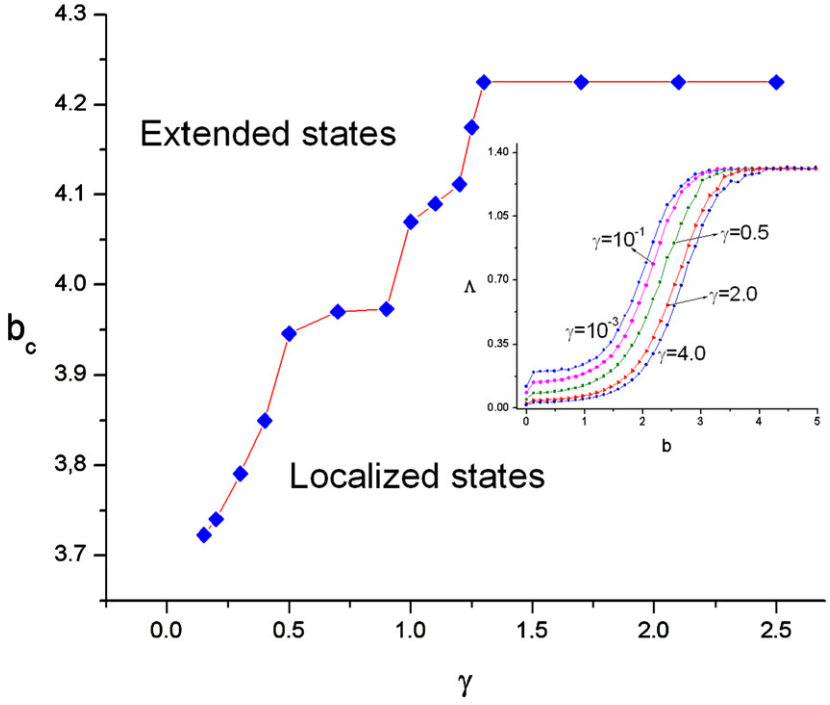

Fig. 5. Phase diagram (γ, b_c) separating localized states from extended states in the thermodynamic limit in terms of the map parameter $b_c(\infty)$ for the case $C = 0.3$ as a function of the parameter γ. The inset shows the normalized localization length $\Lambda(b)$ as a function of the map parameter b for $\omega = 3.5$, $N = 40\,000$ and $C = 0.3$, for γ going from $\gamma = 0.001$ to $\gamma = 4.0$.

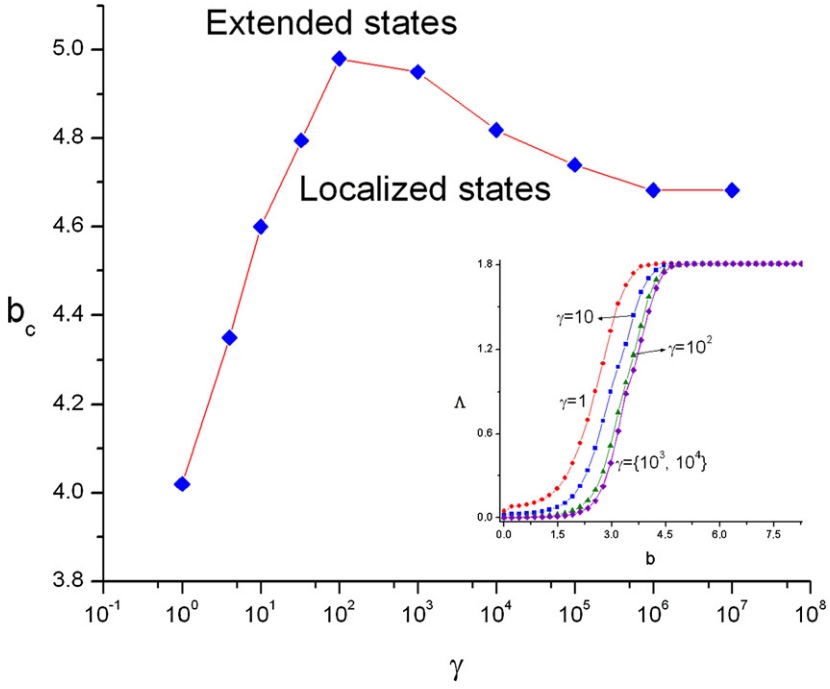

Fig. 6. Phase diagram (γ, b_c) separating localized states from extended states in the thermodynamic limit in terms of the map parameter $b_c(\infty)$ as a function of the parameter γ with $C = (\varepsilon\gamma)^2$ and $\varepsilon = 1$ (limit case). The inset shows the normalized localization length $\Lambda(b)$ as a function of the map parameter b for $\omega = 3.5$ and $N = 40\,000$, for γ going from $\gamma = 1$ to $\gamma = 10^4$, for the same limit case.

for increasing values of the parameter γ and then, b_c does not change.

ii) The limit case: $C = (\varepsilon\gamma)^2$ and $\varepsilon = 1$, with $\gamma \to \infty$.

In this case we study the behavior of the limit case, which occurs when the OU parameters γ and C go to infinity ($\gamma \to \infty$ and $C \to \infty$), in such a way that $\frac{\sqrt{C}}{\gamma} = \varepsilon$ stays constant (we choose $\varepsilon = 1$). The result of Ornstein–Uhlenbeck process without the application of ternary map was shown in Fig. 2. Now, in addition to the OU process we use the ternary map to generate the distribution of capacitances $\{C_j\}$.

Using relation (12), we have found every critical point $b_c(\gamma, C)$ at thermodynamic limit. Fig. 6 shows the phase diagram (γ, b_c), corresponding to this limiting case, with γ ranging from $\gamma = 10^0$ to $\gamma = 10^7$. This phase diagram that separates localized from extended states shows a maximum and, consequently, is very differ-

ent from the phase diagrams of the two cases a) and b), previously studied.

The inset of Fig. 6 shows the behavior of the normalized localization length $\Lambda(b)$ as a function of the parameter b, for fixed frequency $\omega = 3.5$, $N = 40\,000$, for different values of the parameter γ, with $C = (\varepsilon\gamma)^2$ and $\varepsilon = 1$. This picture shows that for each fixed γ value, the normalized localization length $\Lambda(b)$ is a growing function of the map parameter b, until the corresponding saturation point $b = b_s$ appears. This saturation point b_s has a specific value depending on the system size N and the value of the parameter γ, namely, $b_s = b_s(\gamma, N)$, with $C = (\varepsilon\gamma)^2$ and $\varepsilon = 1$. For $b \geqslant b_s$, $\Lambda(b)$ is practically independent of b. In this case we can see two types of behavior for b_s. For low γ ($\gamma \leqslant 10^2$), b_s increases with increasing γ, but for high values of γ ($\gamma \geqslant 10^3$), b_s diminishes with increasing γ, and then, b_s seems not to change. This behavior suggest the existence of a maximum in the relation b_s versus γ. In concordance with this behavior, the critical value b_c at thermodynamic limit (the phase diagram of Fig. 6) also presents a maximum. This phase diagram separates the localized states from the extended states, when the capacitances are distributed according to a ternary map. This phase diagram is one of the main result of this work and contains all the information about the localized or extended states of the disordered transmission lines in this limit case.

4. Conclusion

In summary, we have studied the behavior of bands of extended and localized states as a function of the frequency in disordered classical transmission lines, when the values of capacitances $\{C_j\}$ are distributed according to a ternary model with long-range correlated disorder. We introduce the disorder by means of the Ornstein–Uhlenbeck process, which depends on two parameters γ and C. The OU sequences have a power spectrum $PS(f) = f^{-m}$, $m > 0$. From these sequences we generate a ternary map using the map parameter b, which adjust the occupancy probability of each possible value of the capacitances $\{C_A, C_B, C_C\}$. For a given correlation, determined by the parameters γ and C of the OU process, the normalized localization length $\Lambda(b, N)$, determined by the ternary map, depends on the map parameter b in a complicated way. This behavior is responsible for the phase transition from localized to extended states of the disordered transmission lines. Using the finite-size scaling method, we find that the phase transition is not a finite size effect, because we were able to calculate each critical map parameter b_c at the thermodynamic limit, for every used parameter γ and C of the OU process. With these data we obtained three phase diagrams for the ternary map for the following two different cases: i) γ and C vary independently, and ii) γ and C are related by $C = (\varepsilon\gamma)^2$, with $\varepsilon = 1$ and $\gamma \to \infty$ (the limit case). This is one of the fundamental result of this work. In addition, this work can be compared to a previous work where we studied the disordered transmission lines using the FFM to generate the long-range correlation in ternary maps. The change in the methodology to generate long-range correlation, produces remarkable changes in the shape of the phase diagrams, because the OU process depends on two parameters (γ and C), but the FFM depends on one single parameter (the correlation exponent α). However, with both methods we find bands of extended states in the thermodynamic limit.

Acknowledgements

E. Lazo acknowledges the support of this research by the Dirección de Investigación y Extensión Académica de la Universidad de Tarapacá, under project No. 4720-07. E. Diez acknowledges the financial support of this research by the Cariplo Foundation (project QUANTDEV) and by the Spanish Ministry of Science and Innovation (FIS2009-07880, PPT310000-2009-6, PCT310000-2009-3) and Junta de Castilla y León (SA049A10).

References

[1] P.W. Anderson, Phys. Rev. 109 (1958) 1492.
[2] N.F. Mott, W.D. Twose, Adv. Phys. 10 (1961) 107.
[3] J.C. Flores, J. Phys.: Condens. Matter 1 (1989) 8471.
[4] D.H. Dunlap, H.L. Wu, P.W. Philips, Phys. Rev. Lett. 65 (1990) 88;
P.W. Philips, H.-L. Wu, Science 252 (1991) 1805.
[5] E. Lazo, M.E. Onell, Physica B 299 (2001) 173.
[6] W. Zhang, S.E. Ulloa, Phys. Rev. B 69 (2004) 153203.
[7] M. Titov, H. Schomerus, Phys. Rev. Lett. 95 (2005) 126602.
[8] J.M. Luck, Phys. Rev. B 39 (1989) 5834.
[9] F.A.B.F. de Moura, M.L. Lyra, Phys. Rev. Lett. 81 (1998) 3735;
F.A.B.F. de Moura, M. Lyra, Physica A (Amsterdam) 266 (1999) 465.
[10] J.W. Kantelhardt, S. Russ, A. Bunde, S. Havlin, I. Webman, Phys. Rev. Lett. 84 (2000) 198.
[11] F.M. Izrailev, A.A. Krokhin, Phys. Rev. Lett. 82 (1999) 4062;
F.M. Izrailev, A.A. Krokhin, S.E. Ulloa, Phys. Rev. B 63 (2001) 041102(R);
F.M. Izrailev, N.M. Makarov, J. Phys. A 38 (2005) 10613.
[12] P. Carpena, P.B. Galvan, P.Ch. Ivanov, H.E. Stanley, Nature 418 (2002) 955;
P. Carpena, P.B. Galvan, P.Ch. Ivanov, H.E. Stanley, Nature 421 (2003) 764.
[13] H. Shima, T. Nomura, T. Nakayama, Phys. Rev. B 70 (2004) 075116;
H. Shima, T. Nakayama, Microelectronic J. 36 (2005) 422.
[14] A. Esmailpour, M. Esmaeilzadeh, E. Faizabadi, P. Carpena, M. Reza Rahimi Tabar, Phys. Rev. B 74 (2006) 024206;
A. Esmailpour, H. Cheraghchi, P. Carpena, M. Reza Rahimi Tabar, J. Stat. Mech. (2007) P09014.
[15] T. Kaya, Eur. Phys. J. B 55 (2007) 49.
[16] R. Benhenni, K. Senouci, N. Zekri, R. Bouamrane, arXiv:0906.2402v2 [cond-mat].
[17] Y. Zhao, S. Duan, W. Zhang, arXiv:0908.3871v1 [cond-mat].
[18] E. Abrahams, P.W. Anderson, D.G. Licciardello, T.V. Ramakrishnan, Phys. Rev. Lett. 42 (1979) 673.
[19] E. Díaz, A. Rodríguez, F. Domínguez-Adame, V.A. Malyshev, Europhys. Lett. 72 (2005) 1018.
[20] U. Kulh, F.M. Izrailev, A.A. Krokhin, H.-J. Stöckmann, Appl. Phys. Lett. 77 (2000) 633.
[21] V.A. Yampol'skii, S. Savelev, O.V. Usatenko, S.S. Melnik, F. Kusmartsev, A.A. Krokhin, F. Nori, Phys. Rev. B 75 (2007) 014527.
[22] V. Bellani, E. Diez, R. Hey, L. Toni, L. Tarricone, G.B. Parravicini, F. Dominguez-Ademe, R. Gómez-Alcalá, Phys. Rev. Lett. 82 (1999) 2159.
[23] E. Lazo, E. Diez, Phys. Lett. A 374 (2010) 3538.
[24] C.-K. Peng, S. Havlin, M. Schwartz, H.E. Stanley, Phys. Rev. A 44 (1991) 2239;
H.A. Makse, S. Havlin, M. Schwartz, H.E. Stanley, Phys. Rev. E 53 (1996) 5445.
[25] P. Langevin, Comptes Rendus Acad. Sci. (Paris) 146 (1908) 530.
[26] G.E. Uhlenbeck, L.S. Ornstein, Phys. Rev. 36 (1930) 823.
[27] S. Chandrasekhar, Rev. Mod. Phys. 15 (1943) 1.
[28] Ming Chen Wang, G.E. Uhlenbeck, Rev. Mod. Phys. 17 (1945) 323.
[29] N.G. van Kampen, Stochastic Process in Physics and Chemistry, North-Holland, Amsterdam, 1992;
C.W. Gardiner, Handbook of Stochastic Methods for Physics, Chemistry and the Natural Sciences, Springer-Verlag, Berlin, 1985;
D.T. Gillespie, Markov Process: an Introduction for Physical Scientist, Academic, New York, 1992;
D.T. Gillespie, Am. J. Phys. 64 (1996) 225.
[30] D.T. Gillespie, Phys. Rev. E 54 (1996) 2084.
[31] M.E. Fisher, in: M.S. Green (Ed.), Critical Phenomena, Proceeding of the International School of Physics Enrico Fermi, Course 51, Academic Press, New York, 1971.
[32] E. Brézin, J. Phys. (Paris) 43 (1982) 15.
[33] X.S. Chen, V. Dohm, A.L. Talapov, Physica A 232 (1996) 375;
X.S. Chen, V. Dohm, A.N. Schultka, Phys. Rev. Lett. 77 (1996) 3641.
[34] Ch. Lizhu, X.S. Chen, W. Yuanfang, arXiv:0904.1040v1 [nucl-th].